International Journal of Computer Vision (2020) 128:2325–2343
https://doi.org/10.1007/s11263-020-01326-x

Product Quantization Network for Fast Visual Search

Tan Yu[1] · **Jingjing Meng**[2] · **Chen Fang**[3] · **Hailin Jin**[3] · **Junsong Yuan**[2]

Received: 8 March 2019 / Accepted: 30 March 2020 / Published online: 23 April 2020

Abstract
Product quantization has been widely used in fast image retrieval due to its effectiveness of coding high-dimensional visual features. By constructing the approximation function, we extend the hard-assignment quantization to soft-assignment quantization. Thanks to the differentiable property of the soft-assignment quantization, the product quantization operation can be integrated as a layer in a convolutional neural network, constructing the proposed product quantization network (PQN). Meanwhile, by extending the triplet loss to the asymmetric triplet loss, we directly optimize the retrieval accuracy of the learned representation based on asymmetric similarity measurement. Utilizing PQN, we can learn a discriminative and compact image representation in an end-to-end manner, which further enables a fast and accurate image retrieval. By revisiting residual quantization, we further extend the proposed PQN to residual product quantization network (RPQN). Benefited from the residual learning triggered by residual quantization, RPQN achieves a higher accuracy than PQN using the same computation cost. Moreover, we extend PQN to temporal product quantization network (TPQN) by exploiting temporal consistency in videos to speed up the video retrieval. It integrates frame-wise feature learning, frame-wise features aggregation and video-level feature quantization in a single neural network. Comprehensive experiments conducted on multiple public benchmark datasets demonstrate the state-of-the-art performance of the proposed PQN, RPQN and TPQN in fast image and video retrieval.

Keywords Product quantization · Image retrieval · Deep learning · Video retrieval

1 Introduction

Visual search has been a fundamental research topic in computer vision. Given a query (an image or a video), it aims to retrieve the query's relevant items from a database. Accuracy and efficiency are two key aspects for a retrieval system. These two aspects drive the research on visual search to progress in two directions.

The first direction focuses on representation designing or learning for a higher search accuracy (Philbin et al. 2007; Perronnin et al. 2010; Jégou et al. 2010; Babenko et al. 2014; Babenko and Lempitsky 2015; Ng et al. 2015; Gordo et al. 2016; Yu et al. 2017c; Bai et al. 2018, 2017). A good representation maintains a large distance between irrelevant items in feature space and a close distance between relevant ones. Traditional retrieval systems first extract hand-crafted local features like SIFT and then aggregate local features into a global feature (Philbin et al. 2007; Perronnin et al. 2010; Jégou et al. 2010). With the progress of deep learning, the convolutional neural network provides an effective representation (Babenko et al. 2014; Babenko and Lempitsky 2015; Ng et al. 2015; Yu et al. 2017a, d), which is trained by the semantic information and thus is robust to low-level image transformations.

Communicated by Li Liu, Matti Pietikäinen, Jie Qin, Jie Chen, Wanli Ouyang, Luc Van Gool.

✉ Tan Yu
tyu008@e.ntu.edu.sg

Jingjing Meng
jmeng2@buffalo.edu

Chen Fang
cfang@adobe.com

Hailin Jin
hljin@adobe.com

Junsong Yuan
jsyuan@buffalo.edu

[1] Cognitive Computing Lab, Baidu Research, Seattle, USA

[2] Computer Science and Engineering Department, University at Buffalo, State University of New York, New York, USA

[3] Adobe Research, San Jose, USA

The second direction aims to boost the retrieval speed, especially when dealing with a large-scale dataset. In this circumstance, a compact visual representation is necessary. Generically speaking, there are two types of schemes to gain a compact representation, hashing and quantization. Hashing maps the real-value vectors into binary codes, which enables a faster distance computation and lower memory cost. One of widely used hashing methods is locality sensitivity hashing (LSH) (Charikar 2002). Nevertheless, LSH is data-independent, which ignores the data distribution and is sub-optimal to a specific dataset. To further improve the performance, some hashing methods (Salakhutdinov and Hinton 2007; Weiss et al. 2009; Gong et al. 2013) learn the projection from the data, which caters better to a specific dataset and achieves a higher retrieval precision. Note that traditional hashing methods are based on a two-step procedure. To be specific, they first conduct feature extraction and then carry on Hamming embedding based on the extracted features. These two steps are independently conducted and their mutual influence are ignored. More recently, inspired by the progress of deep learning, some deep hashing methods (Xia et al. 2104; Lai et al. 2015; Liu et al. 2016; Li et al. 2017) are proposed, which simultaneously conduct feature learning and feature compression through a unified neural network, achieving much better retrieval performance compared with methods based on off-the-shelf features.

Nevertheless, hashing methods are only able to produce a few distinct distances, limiting its discriminative power in characterizing distances between data points. In parallel to hashing methods, another widely used data compression method in visual retrieval is product quantization. It quantizes each feature vector into a Cartesian product of several codewords and the similarity can be efficiently computed through looking up cached similarity table. Thanks to the asymmetric distance calculation mechanism, product quantization enables a more accurate distance calculation than hashing methods using the same code length. The product quantization (PQ) (Jegou et al. 2011) and its optimized versions like OPQ (Ge et al. 2013), CKmeans (Norouzi and Fleet 2013), APQ (Babenko and Lempitsky 2014) and CQ (Zhang et al. 2014; Hong et al. 2018) are originally designed for unsupervised scenarios where no labeled data are provided. SQ (Wang et al. 2016c) extends product quantization to supervised scenarios. However, SQ is based on the handcrafted features or CNN features from the pretrained model, therefore it might not be optimal with respect to a specific dataset.

To jointly optimize feature learning and product quantization, Cao et al. (2016) propose a deep quantization network (DQN) which supports an end-to-end training. It optimizes a weighted sum of similarity preserving loss and product quantization loss. It iteratively updates codewords and other parameters of a neural network. Therefore, in each iteration,

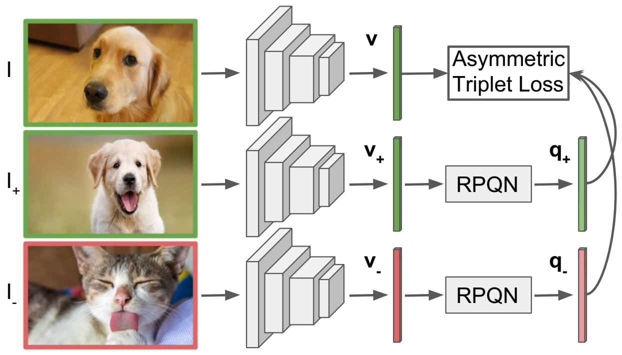

Fig. 1 The architecture of the proposed residual product quantization network (RPQN). It takes triplets as input. Each triplet consists of an anchor image I, a positive image I_+ and a negative image I_-. It obtains real-value feature vectors $[\mathbf{v}, \mathbf{v}_+, \mathbf{v}_-]$ through backbone and further generates soft-quantized representations for positive image and negative image, $[\mathbf{q}_+, \mathbf{q}_-]$, by residual product quantization layer (RPQN). $[\mathbf{v}, \mathbf{q}_+, \mathbf{q}_-]$ constructs asymmetric triplet loss to train the network

the codewords are directly updated by k-means whereas the label information is ignored. Recently, Klein and Wolf (2017) propose a deep product quantization (DPQ). They learn a cascade of two fully-connected layers followed by a softmax layer to determine a soft codeword assignment. It is different from original product quantization as the codeword assignment is no longer determined by distance between the original feature and codewords. Nevertheless, the additional parameters introduced in the cascade of fully-connected layers make DPQ more prone to over-fitting.

In this paper, we also attempt to incorporate the product quantization in a neural network and train it in an end-to-end manner. We construct a soft product quantization layer through an approximation function $f(\mathbf{x}, \alpha)$, which is differentiable and supports an end-to-end training. The original product quantization function $q(\mathbf{x})$ is a special case of the constructed approximation function when $\alpha \rightarrow +\infty$. Different from DPQ, fully-connected layers are no longer needed for codebook assignment, instead, in our method, the codeword assignment is determined by the similarity between features and the codewords. Therefore, we significantly reduce the number of parameters to be trained, making our product quantization network (PQN) less prone to over-fitting compared with DPQ. Meanwhile, inspired by the success of the triplet loss in metric learning and the advantage of the asymmetric similarity measurement in feature compression, we propose a novel asymmetric triplet loss to directly optimize the representation's adaptability to asymmetric similarity measurement in an end-to-end manner. Interestingly, our experiments show that product quantization not also boosts retrieval efficiency, but also serves as a regularization approach, which improves the model's generalizability and improves the retrieval precision.

Meanwhile, we revisit the residual quantization and extend PQN to residual product quantization network (RPQN). In general, residual quantization cannot achieve comparable distortion error as product quantization, which limits its effectiveness in retrieval based on hand-crafted features. Nevertheless, there are large redundancy in features obtained from deep neural network and thus the quantization error is less important. Benefited from residual learning triggered through residual quantization, the proposed RPQN achieves a higher accuracy than PQN. Figure 1 visualizes the architecture of the proposed RPQN. It takes a triplet consisting of an achor image, a positive image and a negative image $[I, I_+, I_-]$ as input. The backbone network, e.g., AlexNet, obtains the images' real-value feature vectors $[\mathbf{v}, \mathbf{v}_+, \mathbf{v}_-]$. The feature vectors of the positve image and negative image are further feed in the proposed residual product quantization layer (RPQL) to generate their quantized features $[\mathbf{q}_+, \mathbf{q}_-]$. The anchor image's real-value feature and the quantized features of the negative image and the positive image constitutes a triplet $[\mathbf{v}, \mathbf{q}_+, \mathbf{q}_-]$ to compute the assymetric loss which aims to enlarge the distance between $\mathbf{v}$ and $\mathbf{q}_-$, and decrease the distance between $\mathbf{v}$ and $\mathbf{q}_+$.

Moreover, we extend PQN to temporal product quantization network (TPQN) by exploiting the temporal consistency inherited in videos through a temporal pyramid pooling. The temporal pyramid pooling not only enhances the discriminativeness of the video representation but also provides a natural feature partition for product quantization. It integrates frame feature learning, frame features aggregation and video feature product quantization in a single neural network.

This paper is an extension of our conference paper (Yu et al. 2018). New contributions are summarized as follows:

- We give a deeper insight into making the quantization differentiable. We propose to construct a function to approximate the hard quantization to achieve the functionality of the quantization. The softmax function used in the original conference paper (Yu et al. 2018) is a special case of the proposed approximation function in this paper. We give a more detailed derivation for the gradient back-propagation and conduct a more comprehensive ablation study.
- We extend the proposed product quantization network (PQN) in the conference paper to residual product quantization network (RPQN) by revisiting the residual quantization. The residual quantization not only brings a finer feature space partition but also triggers the residual learning, enhancing the representation's discriminability. We conduct comprehensive experiments on RPQN and demonstrate that it achieves higher accuracies than the PQN proposed in our conference paper.
- We tackle a new task, video retrieval. By exploiting the temporal consistency inherited in videos, we extend the PQN proposed in our conference paper to temporal product quantization (TPQN). The proposed TPQN integrates frame feature learning, frame features pooling and video feature compression in a single network. We conduct systematic experiments based on the proposed TPQN and achieve state-of-the-art performance in video retrieval task.

The remainder of the paper is organized as follows: Related work for Hashing, quantization and fast video retrieval are discussed in Sect. 2. Product quantization network (PQN) is introduced in Sect. 3. The proposed residual product quantization network (RPQN) is introduced in Sect. 4 and temporal product quantization network (TPQN) is introduced in Sect. 5. Sections 6 and 7 provide experimental results in fast image retrieval and video retrieval, respectively.

2 Related Work

2.1 Hashing

Hashing (Charikar 2002; Salakhutdinov and Hinton 2007; Weiss et al. 2009; Gong et al. 2013; Xia et al. 2104; Lai et al. 2015; Liu et al. 2016; Li et al. 2017; Hong et al. 2017; Hong and Yuan 2018; Hong et al. 2018; Yu et al. 2017b) aims to map a feature vector into a short code consisting of a sequence of bits, which enables fast distance computation as well as small memory cost. One of traditional hashing methods, locality sensitivity hashing (LSH) (Charikar 2002), directly utilizes random projection to map the real-value vectors into binary codes. Since the random projection in LSH is independent with data distribution, it might not be optimal for a specific dataset. To optimize the projection for a specific dataset, spetral hashing (SH) (Weiss et al. 2009) and iterative quantization (ITQ) (Gong et al. 2013) learn the projection by minimizing the distortion errors in an unsupervised manner. They achieve better performance than LSH. To further exploit the supervision information, some supervised hashing methods (Liu et al. 2012; Norouzi et al. 2012; Shen et al. 2015) are proposed, achieving better performance than their unsupervised counterpart such as ITQ and SH.

Nevertheless, the above-mentioned hashing methods all adopt a two-step procedure. They first obtain real-value image features and then compress the features into binary codes. In that case, the representation learning and feature compression are conducted separately and the mutual influence between them is ignored. Recently, motivated by the success of deep learning, some works (Xia et al. 2104; Lai et al. 2015; Liu et al. 2016; Li et al. 2017) propose deep hashing methods by incorporating hashing as a layer into a deep neural network. The end-to-end training mechanism of deep hashing simultaneously optimizes the representation learning and feature compression, achieving better performance than traditional hashing methods based on the two-step procedure.

2.2 Product Quantization

Since the hashing methods are only able to produce a few distinct distances, it has limited capability of describing the distance between data points. Parallelly, another scheme termed product quantization (PQ) (Jegou et al. 2011) possesses a more powerful representation capability. It decomposes the space into a Cartesian product of subspaces and quantizes each subspace individually. Thanks to the product settings, it could partition the feature space into a huge number of fine cells. By utilizing the asymmetric similarity measurement, it only causes quantization error in reference images' features and uses the original feature of the query without any distortion. Meanwhile, through looking up tables, it achieves comparable search speed as Hashing methods. Some following work (Ge et al. 2013; Babenko and Lempitsky 2014; Zhang et al. 2014) further optimize the product quantization through reducing the distortion and achieve higher retrieval precision and recall. Note that, production quantization and its optimized versions such as OPQ (Ge et al. 2013), AQ (Babenko and Lempitsky 2014) and CQ (Zhang et al. 2014) are designed for unsupervised scenarios where no supervision is provided, limiting their effectiveness in the supervised scenario.

To exploit the labels provided in the supervised scenario, Wang et al. (2016c) propose supervised quantization (SQ). Nevertheless, SQ conducts feature extraction and quantization individually, whereas the interaction between these two steps are ignored. To simultaneously learn image representation and product quantization, deep quantization network (DQN) (Cao et al. 2016) adds a fully connected bottleneck layer in the convolutional network. It optimizes a combined loss consisting of a similarity-preserving loss and a product quantization loss. Nevertheless, the codebook in DPQ is trained through k-means clustering and thus the supervision is ignored. Recently, deep product quantization (DPQ) (Klein and Wolf 2017) is proposed where the codebook and network parameters are learned in an end-to-end manner. Different from original product quantization which determines the codeword assignment according to distances between features and codewords, DPQ determines the codeword assignment through a fully connected layer with parameters learned from data. Nevertheless, the additional parameters in the cascade of fully connected layers make the network more prone to over-fitting.

Our work is also an attempt of incorporating product quantization in a neural network. We propose a soft product quantization layer and build our product quantization network (PQN), which can be trained in an end-to-end manner. Different from DPQ, our PQN determines the codeword assignment according to the similarity between features for coding and codewords, which can be seen as a soft extension of original product quantization. Unlike DPQ, we do not need additional fully-connected layers to determine the codeword assignment and the only parameters in our soft product quantization layer are codewords. Therefore, ours is less prone to over-fitting. Besides, we exploit residual quantization besides product quantization in RPQN. The residual quantization triggers the residual learning, which boosts the representation's discriminabilty. Moreover, we extend product quantization to temporal product quantization for speeding up video retrieval. The temporal pyramid used in temporal product quantization not only provides a natural feature partition but also enhances the representation's discriminabilty.

2.3 Fast Video Search

Traditional fast video search methods (Cao et al. 2012; Ye et al. 2013) follow a two-step pipeline by extracting the video feature (Tu et al. 2018, 2019) followed by the feature compression. Nevertheless, this two-step pipeline ignores the interaction between two steps, feature learning and compression, and thus the obtained compact video representation might be sub-optimal. To improve the performance of learned compact code, Wu et al. (2017b) propose a deep video hashing method which jointly optimize frame feature learning and hashing. Similarly, Liong et al. (2017) incorporate video feature learning and hashing function optimization in a single neural network. Recently, Liu et al. (2017) propose a deep video hashing framework as well as a category mask to increase the discriminativity of hash codes. Different from these deep hashing methods, we exploit product quantization to obtain a compact video representation and incorporate it in a neural network. Thanks to asymmetric distance measurement, product quantization results in a smaller distortion error than hashing. Moreover, we exploit the temporal consistency inherited in videos and extend the product quantization to temporal product quantization, constructing the proposed temporal product quantization network (TPQN).

3 Product Quantization Network

3.1 Limitation of Product Quantization

Let us denote by $\mathbf{v} \in \mathbb{R}^d$ the feature of a reference image I, we divide the feature $\mathbf{v}$ into M subvectors $[\mathbf{v}_1, \ldots, \mathbf{v}_m, \ldots, \mathbf{v}_M]$

in the feature space where $\mathbf{v}_m \in \mathbb{R}^{d/M}$ is a subvector. The product quantization further approximates $\mathbf{v}$ by

$$\mathbf{q} = [q_1(\mathbf{v}_1), \ldots, q_m(\mathbf{v}_m), \ldots, q_M(\mathbf{v}_M)], \tag{1}$$

where $q_m(\cdot)$ is m-th quantizer defined as

$$q_m(\mathbf{v}_m) = \mathbf{c}_m^{k^*}, \tag{2}$$

in which,

$$k^* = \underset{k\in[1,K]}{\operatorname{argmax}} \langle \mathbf{v}_m, \mathbf{c}_m^k \rangle. \tag{3}$$

In Eq. (3), $\{\mathbf{c}_m^1, \ldots, \mathbf{c}_m^K\}$ are codewords for $q_m(\cdot)$. Originally, the codewords are learned through unsupervised k-means by minimizing the distortion error between each data point and its nearest codeword. Nevertheless, only minimizing distortion errors between data points and codewords ignores the supervision information. To exploit the provided supervision when incorporated product quantization in a neural network, we seek to learn the codewords through back-propagation in a end-to-end manner.

Let us attempt to derive the back-propagation of gradients in product quantization operation. We define L as the training loss, which we will introduce in Sect. 3.5. Let us assume we have already obtained $\partial L/\partial q_m(\mathbf{v}_m)$, *i.e.*, the derivative of loss $\mathcal{L}$ with respective to the output. The back-propagation seeks to compute the derivative of loss $\mathcal{L}$ with respective to the codewords, $\partial L/\partial \mathbf{c}_m^{k^*}$, and the derivative of loss $\mathcal{L}$ with respective to the input, $\partial L/\partial \mathbf{v}_m$. From the definition, it is straightforward to derive that $\partial L/\partial \mathbf{c}_m^{k^*} = \partial L/\partial q_m(\mathbf{v}_m)$. Intuitively, it back-propagates the gradients of the output to the codewords it is assigned to and leave the other codewords unchanged. Nevertheless, $q_m(\mathbf{v}_m)$ is not a continuous function of $\mathbf{v}_m$, making it infeasible to back-propagate $\partial L/\partial q_m(\mathbf{v}_m)$ to $\partial L/\partial \mathbf{v}_m$. It drives us to seek other solutions to make the back-propagation in product quantization feasible.

3.2 From Hard Quantization to Soft Quantization

To overcome the non-differentiable problem, we generalize the quantization defined in Eq. (2) by constructing a continuously differential approximation function defined as $f_m(\mathbf{v}_m, \alpha)$ which satisfies $\lim_{\alpha\to+\infty} f_m(\mathbf{v}_m, \alpha) = q_m(\mathbf{v}_m)$, where α is a scalar controlling the consistency between $f_m(\mathbf{v}_m, \alpha)$ and $q_m(\mathbf{v}_m)$. In practice, we can choose a large α to achieve a good approximation. There are multiple choices to construct the function $f_m(\mathbf{v}_m, \alpha)$. Below we specify two instances and the soft quantization function proposed in our conference paper (Yu et al. 2018) corresponds to the second one:

$$\begin{aligned} f_m^1(\mathbf{v}_m, \alpha) &= \sum_{k=1}^K \frac{\langle \mathbf{v}_m, \mathbf{c}_m^k\rangle^\alpha}{\sum_{k'=1}^K \langle \mathbf{v}_m, \mathbf{c}_m^{k'}\rangle^\alpha} \mathbf{c}_m^k, \\ f_m^2(\mathbf{v}_m, \alpha) &= \sum_{k=1}^K \frac{e^{\alpha\langle \mathbf{v}_m, \mathbf{c}_m^k\rangle}}{\sum_{k'=1}^K e^{\alpha\langle \mathbf{v}_m, \mathbf{c}_m^{k'}\rangle}} \mathbf{c}_m^k \end{aligned} \tag{4}$$

Note that, $\lim_{\alpha\to+\infty} f_m^1(\mathbf{v}_m, \alpha) = q_m(\mathbf{v}_m)$ might not be satisfied if $\langle \mathbf{v}_m, \mathbf{c}_m^k\rangle < 0$. To tackle this issue, we clip $\langle \mathbf{v}_m, \mathbf{c}_m^k\rangle$ to ensure it is non-negative. Below we derive the gradient back-propagation for $f_m^1(\mathbf{v}_m, \alpha)$ and that of $f_m^2(\mathbf{v}_m, \alpha)$ can be derived in a similar manner. To facilitate the derivation, we introduce a series of intermediate variables $\{a_m^k\}_{m=1,k=1}^{M,K}$ defined as

$$a_m^k = \langle \mathbf{v}_m, \mathbf{c}_m^k\rangle^\alpha / \sum_{k'=1}^K \langle \mathbf{v}_m, \mathbf{c}_m^{k'}\rangle^\alpha. \tag{5}$$

Meanwhile, let us define $\mathbf{q}_m = f_m^1(\mathbf{v}_m, \alpha)$ as output of the approximation function taking $\mathbf{v}_m$ as input. By plugging Eq. (5) into Eq. (4), we can obtain

$$\mathbf{q}_m = \sum_{k=1}^K a_m^k \mathbf{c}_m^k. \tag{6}$$

Since $\mathbf{q}_m$ is a function of $\mathbf{v}_m$ and $\{\mathbf{c}_m^k\}_{k=1}^K$, it is straightforward to obtain

$$\begin{aligned} dL &= \sum_{m=1}^M \left(d\mathbf{q}_m\right)^\top \frac{\partial L}{\partial \mathbf{q}_m} \\ &= \sum_{m=1}^M \left(\frac{\partial \mathbf{q}_m}{\partial \mathbf{v}_m} d\mathbf{v}_m + \sum_{k=1}^K \frac{\partial \mathbf{q}_m}{\partial \mathbf{c}_m^k} d\mathbf{c}_m^k\right)^\top \frac{\partial L}{\partial \mathbf{q}_m}. \end{aligned} \tag{7}$$

Meanwhile, according to the definition of $\mathbf{q}_m$ in Eq. (6),

$$\begin{aligned} \frac{\partial \mathbf{q}_m}{\partial \mathbf{v}_m} &= \sum_{k=1}^K \frac{\partial \mathbf{q}_m}{\partial a_m^k}\left(\frac{\partial a_m^k}{\partial \mathbf{v}_m}\right)^\top = \sum_{k=1}^K \mathbf{c}_m^k \left(\frac{\partial a_m^k}{\partial \mathbf{v}_m}\right)^\top, \\ \frac{\partial \mathbf{q}_m}{\partial \mathbf{c}_m^k} &= \sum_{k''=1}^K \frac{\partial \mathbf{q}_m}{\partial a_m^{k''}}\left(\frac{\partial a_m^{k''}}{\partial \mathbf{c}_m^k}\right)^\top + a_m^k \frac{\partial \mathbf{c}_m^k}{\partial \mathbf{c}_m^k} \\ &= \sum_{k''=1}^K \mathbf{c}_m^{k''}\left(\frac{\partial a_m^{k''}}{\partial \mathbf{c}_m^k}\right)^\top + a_m^k \mathbf{I}, \end{aligned} \tag{8}$$

where $\mathbf{I}$ is an identity matrix. By plugging Eq. (8) into Eq. (7), we further obtain

$$dL = \sum_{m=1}^{M} \Bigg\{ \sum_{k=1}^{K} \mathbf{c}_m^k \Big(\frac{\partial a_m^k}{\partial \mathbf{v}_m}\Big)^\top d\mathbf{v}_m + \sum_{k=1}^{K} \Big[\sum_{k''=1}^{K} \mathbf{c}_m^{k''} \Big(\frac{\partial a_m^{k''}}{\partial \mathbf{c}_m^k}\Big)^\top + a_m^k \mathbf{I} \Big] d\mathbf{c}_m^k \Bigg\}^\top \frac{\partial L}{\partial \mathbf{q}_m}. \tag{9}$$

Meanwhile, L is the function of $\mathbf{v}_m$ and $\mathbf{c}_m^k$, therefore,

$$dL = \sum_{m=1}^{M} \Big[\Big(d\mathbf{v}_m\Big)^\top \frac{\partial L}{\partial \mathbf{v}_m} + \sum_{k=1}^{K} \Big(d\mathbf{c}_m^k\Big)^\top \frac{\partial L}{\partial \mathbf{c}_m^k} \Big]. \tag{10}$$

Comparing Eq. (10) with Eq. (9), we obtain

$$\begin{aligned} \frac{\partial L}{\partial \mathbf{v}_m} &= \sum_{k=1}^{K} \frac{\partial a_m^k}{\partial \mathbf{v}_m} \Big(\mathbf{c}_m^k\Big)^\top \frac{\partial L}{\partial \mathbf{q}_m}, \\ \frac{\partial L}{\partial \mathbf{c}_m^k} &= \sum_{k''=1}^{K} \frac{\partial a_m^{k''}}{\partial \mathbf{c}_m^k} \Big(\mathbf{c}_m^{k''}\Big)^\top \frac{\partial L}{\partial \mathbf{q}_m} + a_m^k \frac{\partial L}{\partial \mathbf{q}_m}. \end{aligned} \tag{11}$$

where

$$\begin{aligned} \frac{\partial a_m^k}{\partial \mathbf{v}_m} &= \frac{\alpha \sum_{k'=1}^{K} \langle \mathbf{v}_m, \mathbf{c}_m^{k'} \rangle^{\alpha-1} \langle \mathbf{v}_m, \mathbf{c}_m^{k} \rangle^{\alpha-1} \mathbf{c}_m^k \langle \mathbf{v}_m, \mathbf{c}_m^{k'} \rangle}{(\sum_{k'=1}^{K} \langle \mathbf{v}_m, \mathbf{c}_m^{k'} \rangle^{\alpha})^2} \\ &\quad - \frac{\alpha \sum_{k'=1}^{K} \langle \mathbf{v}_m, \mathbf{c}_m^{k'} \rangle^{\alpha-1} \langle \mathbf{v}_m, \mathbf{c}_m^{k} \rangle^{\alpha-1} \mathbf{c}_m^{k'} \langle \mathbf{v}_m, \mathbf{c}_m^{k} \rangle}{(\sum_{k'=1}^{K} \langle \mathbf{v}_m, \mathbf{c}_m^{k'} \rangle^{\alpha})^2}, \\ \frac{\partial a_m^{k''}}{\partial \mathbf{c}_m^k} &= \frac{\alpha \mathbb{I}(k=k'') \mathbf{c}_m^{k''} \langle \mathbf{v}_m, \mathbf{c}_m^{k''} \rangle^{\alpha-1} \sum_{k'=1}^{K} \langle \mathbf{v}_m, \mathbf{c}_m^{k'} \rangle^{\alpha}}{(\sum_{k'=1}^{K} \langle \mathbf{v}_m, \mathbf{c}_m^{k'} \rangle^{\alpha})^2} \\ &\quad - \frac{\alpha \mathbf{c}_m^{k} \langle \mathbf{v}_m, \mathbf{c}_m^{k} \rangle^{\alpha-1} \langle \mathbf{v}_m, \mathbf{c}_m^{k''} \rangle^{\alpha}}{(\sum_{k'=1}^{K} \langle \mathbf{v}_m, \mathbf{c}_m^{k'} \rangle^{\alpha})^2}. \end{aligned} \tag{12}$$

$\mathbb{I}(k=k') = 1$ only if $k = k'$ otherwise 0. In fact, our experiments in Sect. 6.1.1 show that, $f_m^1(\cdot, \alpha)$ and $f_m^2(\cdot, \alpha)$ achieve comparable performance. For convenience of implementation, we select $f_m^2(\cdot, \alpha)$ as default approximation function.

3.3 Regularization

Interestingly, the quantization mechanism works as a regularization, effectively suppressing over-fitting. Different from traditional regularization method putting constraints on the weights of the network such as ℓ_1/ℓ_2 regularization, quantization, instead, puts constraints on the activations. We will show that even though the quantized features can be seen as an approximation of the original features with inevitable distortion, it achieves a much better retrieval precision than that using the original features.

3.4 Initialization

We initialize the parameters of convolutional layers by fine-tuning a standard convolutional neural network without quantization, e.g., Alexnet, on the specific dataset. Since we adopt inner-product similarity, we add an intra-normalization layer after the fully-connected layer to fine-tune the network to make it compatible with the proposed product quantization network. After that, we extract the features from the fine-tuned neural network and conduct k-means followed by ℓ_2-normalization to obtain the initialized codewords $\{\mathbf{c}_{mk}\}_{k=1,m=1}^{K,M}$ in the soft product quantization layer.

3.5 Asymmetric Triplet Loss

We extend triplet loss originally used in metric learning to asymmetric triplet loss to boost the performance of learned representation in asymmetric similarity measurement. We define (I, I_+, I_-) as a training triplet, where I_+ represents a relevant (positive) image and I_- is an irrelevant (negative) image with respect to I. We denote by $\mathbf{v}$ the feature of I before soft product quantization and denote by $\mathbf{q}_+$ and $\mathbf{q}_-$ the features of I_+ and I_- after soft product quantization. We define asymmetric similarity between I and $I+$ as $\langle \mathbf{v}, \mathbf{q}_+ \rangle$, where $\langle \cdot, \cdot \rangle$ denotes the inner-product between two vectors. The proposed asymmetric triplet loss is defined as

$$\mathcal{L}_{ATL} = \langle \mathbf{v}, \mathbf{q}_- \rangle - \langle \mathbf{v}, \mathbf{q}_+ \rangle. \tag{13}$$

Intuitively, it aims to increase the asymmetric similarity between pairs of relevant images and decrease that of pairs of irrelevant images. It is a natural extension of the original triplet loss to asymmetric distance. The difference is that, a training triplet used in the original triplet loss consists of three features of the same type, whereas a training triplet used in the proposed asymmetric triplet loss consists of one feature without quantization and two features after quantization. In fact, our experiments in Sect. 6.1.1 show that a better performance is achieved by processing the above loss through a sigmoid function and a revised loss function is defined as Eq. (14). The better performance might be attributed to the fact that the sigmoid function can normalize the original loss so that the training will not be biased by some samples with huge loss. By default, the asymmetric triplet loss (ATL) we mention in this paper is $\mathcal{L}_{ATL}^+$ in Eq. (14).

$$\mathcal{L}_{ATL}^+ = \frac{1}{1 + e^{\langle \mathbf{v}, \mathbf{q}_+ \rangle - \langle \mathbf{v}, \mathbf{q}_- \rangle}}. \tag{14}$$

3.6 Encoding and Retrieval

After training the proposed product quantization network, the reference images in the database will be encoded by hard product quantization. We define the layer before the soft product quantization layer as embedding layer. Given a reference image I, we obtain its feature from embedding layer $\mathbf{v} = [\mathbf{v}_1, \ldots, \mathbf{v}_m, \ldots, \mathbf{v}_M]$ and then obtain its PQ code $\mathbf{i} = [i_1, \ldots, i_m, \ldots, i_M]$ where i_m is computed by

$$i_m = \underset{k \in [1,K]}{\operatorname{argmax}} \langle \mathbf{v}_m, \mathbf{c}_m^k \rangle, \tag{15}$$

where $\{\mathbf{c}_m^k\}_{m=1,k=1}^{M,K}$ are codewords learned from our product quantization network. In the retrieval phase, we obtain the query's feature from the embedding layer $\mathbf{v}^q = [\mathbf{v}_1^q, \ldots, \mathbf{v}_m^q, \ldots, \mathbf{v}_M^q]$. The relevance between the query and a reference image represented by its product quantization code $\mathbf{i} = [i_1, \ldots, i_m, \ldots, i_M]$ is computed by the asymmetric similarity $s(\mathbf{v}^q, \mathbf{i})$ defined as

$$s(\mathbf{v}^q, \mathbf{i}) = \sum_{m=1}^{M} \langle \mathbf{v}_m^q, \mathbf{c}_m^{i_m} \rangle. \tag{16}$$

Since $\{\langle \mathbf{v}_m^q, \mathbf{c}_m^k \rangle\}_{k=1}^{K}$ is computed only once for all the reference images in the database and thus obtaining $s(\mathbf{v}^q, \mathbf{i})$ only requires to sum up the pre-computed similarity scores in the look-up table, considerably speeding up the image retrieval process. Meanwhile, storing the product quantization code $\mathbf{i}$ only requires $M \log_2 K$ bits, which considerably reduces the memory cost.

3.7 Relation to Existing Methods

DQN (Cao et al. 2016) is the first attempt of incorporating product quantization in the neural network. It alternately optimizes codewords and other parameters of the network. It is worth noting that when updating codewords, it only minimizes the quantization errors through k-means and the supervision information is ignored.

SUBIC (Jain et al. 2017) integrates the one-hot block encoding layer in the deep neural network. It represents each image by a product of one-hot blocks, following the spirit of product quantization. Nevertheless, the sparse property limits its representation capability, making it perform not as well as ours as shown in Table 11.

DPQ (Klein and Wolf 2017) is another attempt of incorporating product quantization into the neural network. It determines the codeword assignment through a cascade of two fully-connected layers. In contrast, our method determines the codeword assignment according to the similarity between original features and the codewords. Note that, the additional parameters from these two fully-connected layers in DPQ not only increase the computation complexity in training the neural network, but also make the network more prone to over-fitting. Our experiments show that our proposed PQN considerably outperforms DPQ.

4 Residual Product Quantization Network

Different from PQ, residual quantization (RQ) (Chen et al. 2010) performs quantization on the entire feature space, and then recursively applies vector quantization (VQ) to the residuals of the previous quantization level. It is a stacked quantization model. In other words, different from PQ conducting VQ independently on several partitioned sub-spaces, RQ conducts VQ on multiple levels instead. For the first level, RQ simply applies VQ to quantize a feature vector $\mathbf{v}$ into one of K centroids through $q_0(\mathbf{v})$. The feature vector's residual vector $\mathbf{r}_1$ can be obtained by subtracting its corresponding centroid as $\mathbf{v} - q_0(\mathbf{v})$. After than, $\mathbf{r}_1$ will be further quantized into K centroids through $q_1(\mathbf{r}_1)$. By repeatedly quantizing the residuals $M_r - 1$ times, we can approximate $\mathbf{v}$ by $q_0(\mathbf{v}) + \sum_{m=1}^{M_r-1} q_m(\mathbf{r}_m)$. Through combining codewords in M_r levels, we obtain a considerably huge codebook consisting of K^{M_r} codewords. Generally, residual quantization cannot achieve comparable distortion error as product quantization, which limits its effectiveness in retrieval based on off-the-shelf features.

Nevertheless, in a deep learning network, there existing huge amount of redundancy in activations and the quantization error is less important. Meanwhile, we observe that the residual quantization naturally triggers residual learning (He et al. 2016), which can boost the features' discriminability. Based on the above motivation, we attempt to integrate the residual quantization in a deep neural network. We demonstrate the advantage of residual quantization over product quantization when incorporated into a deep neural network. In fact, the residual quantization in our framework not only minimizes the distortion error caused by the quantization, but more importantly, it triggers residual learning and enhances the discriminability of the learned compact representation.

4.1 Residual Product Quantization Layer

Figure 2 illustrates the proposed residual product quantization layer (RPQL). In this case, we set the residual level $M_r = 2$. We denote by $\mathbf{v} \in \mathbb{R}^d$ the input feature vector. RPQL divides $\mathbf{v}$ into M_p sub-vectors:

$$\mathbf{v} \rightarrow [\mathbf{v}_1, \ldots, \mathbf{v}_m, \ldots, \mathbf{v}_{M_p}] \tag{17}$$

For each sub-vector $\mathbf{v}_m$, it goes through the following forward path:

1. $\mathbf{q}_m^1 \leftarrow f(\mathbf{v}_m, \alpha)$

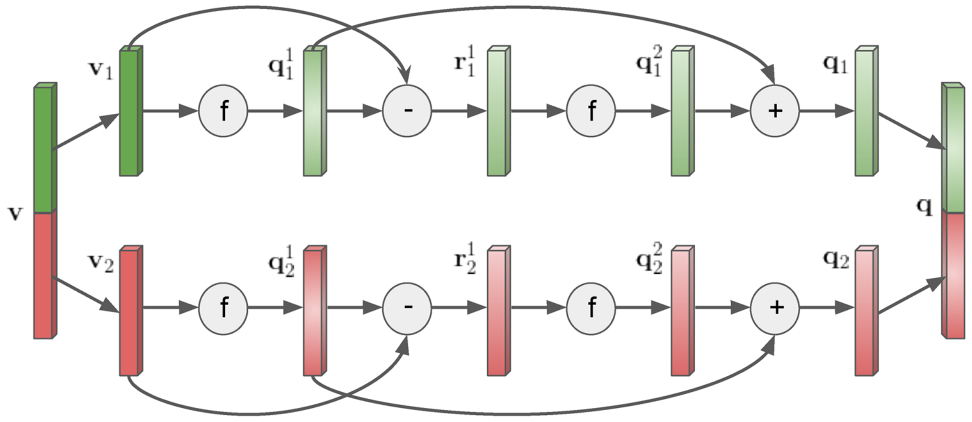

Fig. 2 The architecture of the proposed residue product quantization layer. It splits the real-value feature $\mathbf{v}$ to sub-features $[\mathbf{v}_1, \mathbf{v}_2]$. Through approximation function $f(\cdot, \alpha)$, each sub-feature $\mathbf{v}_m$ is quantized into $\mathbf{q}_m^1$ and then obtains the first-level residual vector $\mathbf{r}_m^1 \leftarrow \mathbf{x}_m - \mathbf{q}_m^1$. Each residual vector $\mathbf{r}_m^1$ is further quantized into $\mathbf{q}_m^2$. After that, $\mathbf{q}_m^1$ and $\mathbf{q}_m^2$ are summed up to obtain the $\mathbf{q}_m$. $\mathbf{q}_1$ and $\mathbf{q}_2$ are concatenated into $\mathbf{q}$

2. $\mathbf{r}_m^1 \leftarrow \mathbf{v}_m - \mathbf{q}_m^1$
3. $\mathbf{q}_m^2 \leftarrow f(\mathbf{r}_m^1, \alpha)$
4. $\mathbf{q}_m \leftarrow \mathbf{q}_m^1 + \mathbf{q}_m^2$

where $f(\cdot, \alpha)$ is the soft function defined in Sect. 3.

4.2 Indexing and Retrieval

After training the network, in the indexing phase, we encode each reference image I in the database through hard-assignment residual product quantization. Let us define the layer before residual product quantization layer as embedding layer. We denote by $\mathbf{v}$ the output of embedding layer when input is I. $\mathbf{v}$ is partitioned into $[\mathbf{v}_1, \ldots, \mathbf{v}_m, \ldots, \mathbf{v}_{M_p}]$ and each sub-vector $\mathbf{v}_m$ is indexed as follows:

1. $i_m^1 \leftarrow \underset{k\in[1,K]}{\text{argmax}} \langle \mathbf{x}_m, \mathbf{c}_m^{1,k} \rangle$
2. $\mathbf{r}_m^1 \leftarrow \mathbf{x}_m - \mathbf{c}_m^{1 i_m^1}$
3. $i_m^2 \leftarrow \underset{k\in[1,K]}{\text{argmax}} \langle \mathbf{r}_m^1, \mathbf{c}_m^{2,k} \rangle$

In the indexing phase, for each reference image I, we only need to store indices of their corresponding codewords $\{i_m^1\}_{m=1}^{M_p}$ and $\{i_m^2\}_{m=1}^{M_p}$, taking $2M_p log_2 K$ bits in total. In the retrieval phase, we utilize the asymmetric similarity scores to rank the reference images in the dataset. Let denote by $\mathbf{v}^q$ the output of embedding layer when the input is query image q. Let denote by $[i_1^1, ..., i_{M_p}^1]$ and $[i_1^2, ..., i_{M_p}^2]$ indices in two-level residual product quantization of the reference image I. The asymmetric similarity is defined as

$$sim_{asym}(q, I) = \sum_{m=1}^{M_p} [\langle \mathbf{v}_q, \mathbf{c}_m^{1,i_m^1} \rangle + \langle \mathbf{v}_q, \mathbf{c}_m^{2,i_m^2} \rangle]. \tag{18}$$

In this case, for each query, we only need to compute its similarity with all the codewords for only once and then similarity between the query and each reference image can be efficiently obtained through $2M_p$ table look-ups.

5 Temporal Product Quantization Network

The proposed PQN and RPQN in the previous section are designed for fast image retrieval and are not optimal for video retrieval task. In this section, we introduce our temporal product quantization network (TPQN) for effective and efficient video retrieval. The proposed TPQN is an extension of the proposed product quantization network by further exploiting the temporal consistency inherited in videos. It integrates frame-wise feature learning, frame-wise features aggregation and video-level feature quantization in a single neural network, and supports an end-to-end training. Figure 3 visualizes the architecture of the proposed TPQN. In Sects. 5.1 and 5.2, we will introduce two core modules of TPQN sequentially. In Sect. 5.3, the indexing and retrieval strategy will be introduced.

5.1 Convolutional and Pooling Layers

Given a video V, we uniformly sample N frames from it and define a global set of sampled frames as $\mathcal{S} = \{f_1, \ldots, f_N\}$. We feed frames $\{f_i\}_{i=1}^N$ in parallel into the backbone network consisting of convolutional and pooling layers and obtain a set of frame-level features $\{F(f_i)|f_i \in \mathcal{S}\}$. We uniformly partition the global set of frames $\mathcal{S}$ into T subsets $\{\mathcal{S}^t\}_{t=1}^T$ where $\mathcal{S}^t = \{f_i | i \in [\lfloor N/T \rfloor (t-1) + 1, \lfloor N/T \rfloor t]\}$. Each subset $\mathcal{S}^t$ represents a continuous interval of the video. Features of frames in each subset $\mathcal{S}^t$ are max-pooled into an interval's feature:

$$\mathbf{v}^t = \text{maxpool}(\{F(f)|f \in \mathcal{S}^t\}), \quad t = 1, \ldots, T+1 \tag{19}$$

where $\mathcal{S}^{T+1} = \mathcal{S}$ accounts for the global set containing all sampled frames. All the interval-level features will be concatenated into a global feature $\mathbf{v} = [\mathbf{v}^1, \ldots, \mathbf{v}^{T+1}]$, which

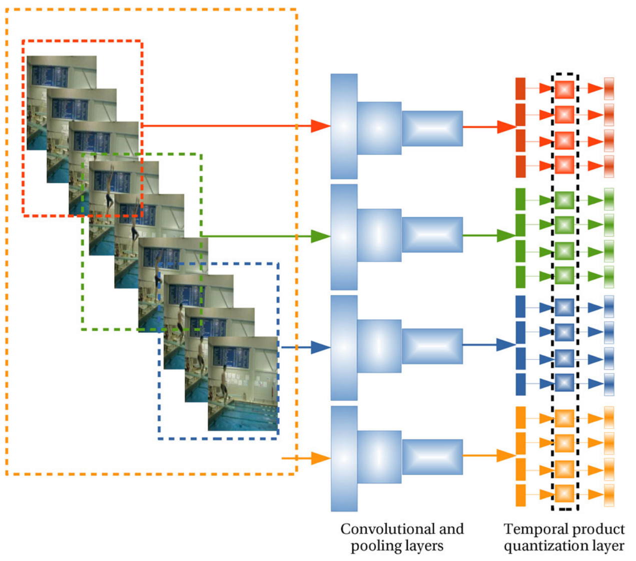
Convolutional and pooling layers
Temporal product quantization layer

Fig. 3 The architecture of the proposed temporal product quantization network (TPQN). The input video V is segmented into multiple intervals. An interval's representation is obtained through convolutional and pooling layers and the video's feature is obtained through temporal pyramid pooling. The temporal product quantization layer takes the obtained representation of the video as input and further conducts soft product quantization

is the input of the proposed temporal product quantization layer. Intuitively, $\mathbf{v}$ is a two-level temporal pyramid pooling feature which exploits the temporal consistency inherited in the videos. But more importantly, the pyramid structure provides a natural feature partition for product quantization.

5.2 Temporal Product Quantization Layer

For each interval-level feature $\mathbf{v}^t$, following the standard product quantization, we equally split it into M sub-vectors as $\mathbf{v}^t = [\mathbf{v}_1^t, \ldots, \mathbf{v}_M^t]$. Each $\mathbf{v}_m^t$ goes through the following pipeline consisting of 4 steps:

1. $\mathbf{y}_{tm} = \text{relu}(\mathbf{W}_m^t \mathbf{v}_m^t + \mathbf{b}_m^t)$
2. $\bar{\mathbf{y}}_m^t = \frac{\mathbf{y}_m^t}{\|\mathbf{y}_m^t\|_2}$
3. $\mathbf{z}_m^t = f_m^t(\bar{\mathbf{y}}_m^t, \alpha)$
4. $\bar{\mathbf{z}}_m^t = \beta \frac{\mathbf{z}_m^t}{\|\mathbf{z}_m^t\|_2}$

where $\mathbf{W}_m^t$ and $\mathbf{b}_m^t$ in step 1 are parameters of a fully-connected layer used to further boost the feature's discriminability. β in step 4 is a scalar to speed up the training and quantizer $f_m^t(\bar{\mathbf{y}}_m^t, \alpha)$ is defined as Eq. 4.

5.3 Indexing and Retrieval

After training the neural network, we will use the learned codewords but adopt hard quantization for indexing. To be specific, given a reference video V in the database, let $\mathbf{v}^t = [\mathbf{v}_1^t, \ldots, \mathbf{v}_m^t, \ldots, \mathbf{v}_M^t]$ denote the max-pooled feature of the intervals I_t where $\mathbf{v}_m^t$ is the m-th sub-vector. For each $\mathbf{v}_m^t$, we obtain its index i_m^t by

1. $\mathbf{y}_m^t = \text{relu}(\mathbf{W}_m^t \mathbf{b}_m^t + \mathbf{b}_m^t)$
2. $\bar{\mathbf{y}}_m^t = \frac{\mathbf{y}_m^t}{\|\mathbf{y}_m^t\|_2}$
3. $i_m^t = \underset{k \in [1,K]}{\text{argmax}} \langle \bar{\mathbf{y}}_m^t, \mathbf{c}_m^{t,k} \rangle$

where K is the number of codewords used by each quantizer $q_m^t(\cdot)$. It takes $log_2(K)$ bits to store i_m^t and $(T+1)Mlog_2(K)$ bits to store all indices $\{[i_1^t, \ldots, i_M^t]\}_{t=1}^{T+1}$ for the video V. The advantage of the proposed temporal product quantization over the original product quantization is that it exploits the temporal consistency inherited in the video, significantly boosting the representation's discriminability.

In the retrieval phase, given a query video q, we can directly obtain its concatenated max-pooled feature $[\mathbf{v}_{q,1}^1, \ldots, \mathbf{v}_{q,M}^{T+1}]$ through the trained backbone network, further post-process each $\mathbf{v}_{q,m}^t$ through $\{\mathbf{W}_m^t, \mathbf{b}_m^t\}$ followed by ℓ_2 normalization and obtain the final feature $[\bar{\mathbf{y}}_{q,1}^1, \ldots, \bar{\mathbf{y}}_{q,M}^{T+1}]$. Note that we do not conduct quantization on the query's feature due to the asymmetric similarity measurement. The similarity between the query q and a reference video V is computed by

$$\text{sim}(q, V) = \sum_{t=1}^{T+1} \sum_{m=1}^{M} \langle \bar{\mathbf{y}}_{q,m}^t, \mathbf{c}_m^{t,i_m^t} \rangle. \tag{20}$$

Computing Eq. (20) is considerably efficient by utilizing look-up table (Jegou et al. 2011). To be specific, we only need to compute the similarity between query video's feature with each codeword $\langle \bar{\mathbf{y}}_{q,m}^t, \mathbf{c}_m^{t,k} \rangle$ for one time and then store the similarity in a look-up table. Computing the similarity between the query video q and a reference video V defined in Eq. (20) only need $M \times (T+1)$ times similarity table look-ups.

We summarize architectures of PQN, RPQN, and TPQN in Table 1.

Table 1 Comparisons between PQN, RPQN, and TPQN

	Product	Residual	Temporal
PQN	✓		
RPQN	✓	✓	
TPQN	✓		✓

PQN adopts the product quantization architecture, RPQN exploits the residual quantization besides the product quantization, and TPQN utilizes the temporal structure besides product quantization

6 Experiments on Image Retrieval

We evaluate the performance of our PQN on two public benchmark datasets, CIFAR-10 and NUS-WIDE. CIFAR-10 (Krizhevsky 2009) is a dataset containing 60,000 color images in 10 classes, and each class has 6000 images in size 32×32. Different from CIFAR-10, NUS-WIDE (Chua et al. 2009) is a dataset for evaluating multi-class classification, in which one sample is assigned to one or multiple labels. We follow the settings in (Lai et al. 2015; Cao et al. 2016) and use the subset of 195,834 images that are associated with the 21 most frequent concepts, where each concept consists of at least 5000 images. We resize all images into 256×256.

On the CIFAR-10 dataset, the performance reported by different baselines are based on different base convolutional neural networks, making it unfair to directly compare their reported retrieval accuracy. To make a fair comparison, we evaluate our method based on two types of convolutional neural networks. The first convolutional neural network we use is 3CNet which is also used by SUBIC (Jain et al. 2017) and DPQ (Klein and Wolf 2017). 3CNet is proposed in Liu et al. (2016), which consists of $L = 3$ convolutional layers with 32, 32 and 64 filters of size 5×5 respectively, followed by a fully connected layer with $d = 500$ nodes. The second convolutional neural network we choose is AlexNet. It is worth noting that the baselines we compare may apply different models. For example, DQN (Cao et al. 2016) adopts AlexNet whereas other work (Wang et al. 2016b; Li et al. 2017) adopt VGG-F model. These two models are similar in the architecture. To be specific, both the CNN-F and AlexNet consist of five convolutional layers and two fully connected layers. As shown in (Jiang and Li 2018), the CNN-F generally performs better than Alexnet in image retrieval, therefore, the better performance of ours based on AlexNet than existing state-of-art methods based on CNN-F is not owing to better base network. In other words, our method can achieve better performance even with an inferior base network. On the NUS-WIDE dataset, we also adopt AlexNet as our base model. On both datasets, we report the performance of the proposed method through mAP, which is a standard metric in evaluating the performance of retrieval algorithms.

6.1 CIFAR-10 Using 3CNet

Following the experimental setup in SUBIC (Jain et al. 2017) and DPQ (Klein and Wolf 2017), the training is conducted on 50K image training set. The test set is split into 9K database images and 1K query images (100 per class).

6.1.1 Ablation Study on PQN

We first evaluate the influence of the number of subvectors M and the number of codewords per sub-codebook K on the retrieval precision of PQN. In experiments, we change M among $\{1, 2, 4, 8\}$, and vary K among $\{2^3, 2^6, 2^9, 2^{12}\}$. As shown in Table 2, PQN achieves the best performance when $M = 4$. By default, we set $M = 4$. Note that when $M \in \{1, 2\}$, the performance of PQN increases as K increases. This is expected since the larger K can partition the feature space into finer cells. Nevertheless, when $M = 4$, the performance drops when K increases from 2^9 to 2^{12}. Meanwhile, when $M = 8$, there is also a performance drop when K increases from 2^6 to 2^9. The worse performance might be caused by over-fitting when both M and K are large. α controls the quantization softness of the soft product quantization layer.

We further evaluate the performance of our method when α varies. We test the influence of α by fixing $M = 4$ and varying K among $\{2^3, 2^6, 2^9, 2^{12}\}$. As shown in Table 3, the performance of the proposed PQN is relatively stable when α increases from 1 to 80. Note that, when $\alpha = 1$, the performance is slightly worse than that when $\alpha = 5$. The worse performance is due to the fact a small α will make the quantization too soft and thus the soft quantization in training phase differs too much from the hard quantization in the testing phase. Meanwhile, we also observe a performance drop when α increases from 5 to 80. This drops might be caused by the fact that a huge α tends to push the input of soft-max function to the saturation region and lead to gradient vanishing. By default, we set $\alpha = 5$.

We compare the $\mathcal{L}_{ATL}$ in Eq. (13) and its sigmoid-version $\mathcal{L}^{+}_{ATL}$ in Eq. (14). As shown in Table 4, $\mathcal{L}^{+}_{ATL}$ achieves slightly better performance than $\mathcal{L}_{ATL}$. The better performance might be attributed to the fact that the sigmoid function can balance the losses of different samples and thus the network training will not be dominated by samples generating huge loss.

Table 2 Influence of M and K on PQN

M	1	2	4	8
$K = 2^3$	0.539	0.650	**0.741**	0.708
$K = 2^6$	0.696	0.741	**0.782**	0.724
$K = 2^9$	0.712	0.750	**0.787**	0.713
$K = 2^{12}$	0.735	0.763	**0.786**	0.737

Bold values indicate the best performance

Table 3 Influence of α on PQN

α	1	5	20	40	80
$K = 2^3$	0.731	**0.741**	0.741	0.732	0.734
$K = 2^6$	0.771	**0.782**	0.782	0.780	0.760
$K = 2^9$	0.779	**0.787**	0.786	0.784	0.780
$K = 2^{12}$	0.785	**0.786**	0.782	0.782	0.781

Bold values indicate the best performance

Table 4 Performance comparisons between $\mathcal{L}_{ATL}$ in Eq. (13) and its sigmoid-version $\mathcal{L}^{+}_{ATL}$ in Eq. (14)

	12 bits	24 bits	36 bits	48 bits
$\mathcal{L}_{ATL}$	0.732	0.773	0.781	0.781
$\mathcal{L}^{+}_{ATL}$	**0.741**	**0.782**	**0.787**	**0.786**

Bold values indicate the best performance

Table 5 Performance comparisons between $f_1(\cdot,\cdot)$ and $f_2(\cdot,\cdot)$ in Eq. (4)

	12 bits	24 bits	36 bits	48 bits
$f_1(\cdot,\cdot)$	**0.745**	**0.784**	0.785	0.783
$f_2(\cdot,\cdot)$	0.741	0.782	**0.787**	**0.786**

Bold values indicate the best performance

Table 6 Comparisons with PQ and LSQ

	8 bits	16 bits	24 bits	32 bits
TL+Full	0.779			
TL+PQ	0.621	0.741	0.773	0.780
TL+LSQ	0.720	0.752	0.753	0.763
PQN	**0.729**	**0.778**	**0.782**	**0.786**

Bold values indicate the best performance

Table 7 Comparisons with other methods in the open-set setting

	8 bits	16 bits	24 bits	32 bits
DTSH (Wang et al. 2016b)	0.261	0.269	0.297	0.341
Triplet + PQ	0.282	0.316	0.332	0.341
DPQ	**0.329**	**0.349**	**0.357**	**0.356**

Bold values indicate the best performance

We compare the performance of two different approximation function $f_1(\cdot,\cdot)$ and $f_2(\cdot,\cdot)$ in Eq. (4). As shown in Table 5, these two approximation functions achieve comparable performance. Considering the complexity of implementation, we select $f_2(\cdot,\cdot)$ as default approximation function.

We compare PQN with unsupervised PQ and LSQ (Martinez et al. 2016) based on fine-tuned features trained through triplet loss. As shown in Table 6, ours considerably outperforms both TL+PQ and TL+LSQ. Meanwhile, we also show the performance of original features trained through triplet loss without quantization (TL+Full) in Table 6. Note that, to make a fair comparison, the triplet loss we used for full feature without quantization is also the revised one as Eq. (14). The performance of ours is even better than that of features without quantization, this is owing to the regularization imposed by quantization, which suppresses over-fitting.

We evaluate the proposed PQN in the open-set setting (Sablayrolles et al. 2017) on CIFAR-10 dataset. In the testing phase, the query and reference images are of different classes from that in the training phase. We train the PQN using samples with labels $c \in [0, 4]$ and conduct the retrieval using samples with labels in $c \in [5, 9]$. In the training data, each class contains 5000 samples. In the testing data, each class contains 1000 classes. Among 5000 testing samples, 1000 samples from the testing data are randomly selected as query and the rest 4000 samples are used as reference images. We compare with DTSH (Wang et al. 2016b) and Triplet + PQ. To be specific, Triplet + PQ is implemented by training the backbone without quantization and then conducted the unsupervised PQ. As shown in Table 7, our method consistently outperforms the DTSH (Wang et al. 2016b) and Triplet + PQ in the open-set setting.

We evaluate the proposed PQN using another two backbones, ResNet34 and ResNet50. The feature dimension of ResNet-34 is 512 and that of the ResNet-50 is 2048. As shown in Table 8, when $M \in \{1, 2\}$, the best performance is achieved when $K = 64$. On the other hand, when $M \in \{4, 8\}$, the best performance is achieved when $K = 16$. Note that, when $K = 256$, the performance is worse than that when $K = 64$. The worse performance might be caused by over-fitting.

We evaluate the influence of the sampling strategy of the triplet loss on the proposed PQN. We compare the uniform sampling, hard negative sampling and distance weighted sampling (Wu et al. 2017a). As shown in Table 9, the hard negative sampling is worse than uniform sampling, and the distance weighted sampling is slightly better than uniform sampling. Considering the effectiveness and simplicity, we use uniform sampling as default.

6.1.2 Ablation Study on RPQN

We then evaluate the influence of residual level M_r on the performance of our RPQN. Note that, when $M_r = 1$, the residual product quantization will degenerate to the product quantization. We compare the case when $M_r = 1$ and that

Table 8 The influence of M and K on the ResNet34 and ResNet50 features

	ResNet34 (512-d)				ResNet50 (2048-d)			
	$K = 4$	$K = 16$	$K = 64$	$K = 256$	$K = 4$	$K = 16$	$K = 64$	$K = 256$
$M = 1$	0.353	0.914	0.914	0.908	0.376	0.918	0.919	0.914
$M = 2$	0.451	0.921	0.924	0.919	0.627	0.928	0.931	0.925
$M = 4$	0.635	0.935	0.930	0.929	0.797	0.938	0.936	0.933
$M = 8$	0.773	0.927	0.924	0.922	0.782	0.931	0.930	0.927

Table 9 Comparisons among different sampling methods

Method	8 bits	16 bits	24 bits	32 bits
Uniform	0.729	0.778	0.782	0.787
Hard Negative	0.632	0.679	0.692	0.701
Distance Weighted	0.733	0.783	0.786	0.788

Table 10 Influence of M_r. When $M_r = 1$, the product residual product quantization degenerates into product quantization

M_r	12 bits	24 bits	36 bits	48 bits
1	0.741	0.782	0.787	0.786
2	**0.758**	**0.799**	**0.796**	**0.797**
4	0.711	0.762	0.765	0.776

Bold values indicate the best performance

when $M_r = 2, 4$. Since the code length $L = M_p M_r log_2 K$, to achieve an identical code length, we set $M_p = 4$ when $M_r = 1$, set $M_p = 2$ when $M_r = 2$, and set $M_p = 1$ when $M_r = 4$. As shown in Table 10, the performance when $M_r = 2$ consistently outperforms others. By default, we set $M_r = 2$ on all testing dataset. Meanwhile, the better performance of $M_r = 2$ than $M_r = 1$ verifies the advantage of residual product quantization over product quantization.

We also evaluate the influence of M_p. In implementation, we fix $M_r = 2$, change M_p among $\{1, 2, 4\}$. We comprehensively test cases when K varies among $\{8, 64, 512, 4096\}$. As shown in Fig. 4, when $M_p = 2$, it achieves the highest mAP on all cases and meanwhile it takes only a half number of bits of that when $M_p = 4$. By default, we set $M_p = 2$.

6.1.3 Compare with State-of-the-Art Methods

We compare the proposed PQN and RPQN with two state-of-the-art methods (SUBIC and DPQ), which adopt the same 3CNet as well as the same experimental settings. We change bit length L among $\{12, 24, 36, 48\}$. We set $M = 4$ on PQN, and set $M_r = 2$ and $M_p = 2$ on RPQN. Since SUBIC adopts cross-entropy loss, it is unfair to directly compare it with ours using asymmetric triplet loss. Therefore, we report the performance of our PQN and RPQN based on the cross-entropy loss (CEL) as well as the proposed asymmetric triplet loss (ATL). As shown in Table 11, our PQN and RPQN based on both CEL and ATL significantly outperform the existing state-of-the-art methods including SUBIC and DPQ.

6.2 CIFAR-10 Using AlexNet

Following the experimental settings in (Wang et al. 2016b; Li et al. 2017), we randomly sample 1000 images per class (10000 images in total) as the testing query images, and the remaining 50000 images are used as the training set as well as reference images in the database. We set $M = 4$ on PQN, and set $M_r = 2$ and $M_p = 2$ on RPQN. We vary K among $\{2^4, 2^6, 2^9, 2^{12}\}$, and thus the code length L varies among $\{16, 24, 36, 48\}$.

6.2.1 Comparions with State-of-the-Art Methods

As shown in Table 12, ours consistently outperforms the existing state-of-the-art methods, especially when the bit length is small. For instance, when the bit length is 16, our PQN/RPQN achieves a 0.947/0.950 mAP whereas DSDH only achieves a 0.935 mAP.

6.2.2 Extremely Short Code Evaluation

As shown in Table 12, the mAP achieved by our method does not drop when the bit length decreases from 48 to 16. In contrast, the performance of other methods in Table 12 all turn worse due to decrease of the bit length. To fully exploit the potential of the proposed product quantization network on the CIAFR-10 dataset, we evaluate it by setting the code length L extremely small. We vary M among 1, 2 and 4, and meanwhile vary the code length (bit number) L within $\{4, 6, 8, 10, 12\}$. As shown in Table 13, when code length

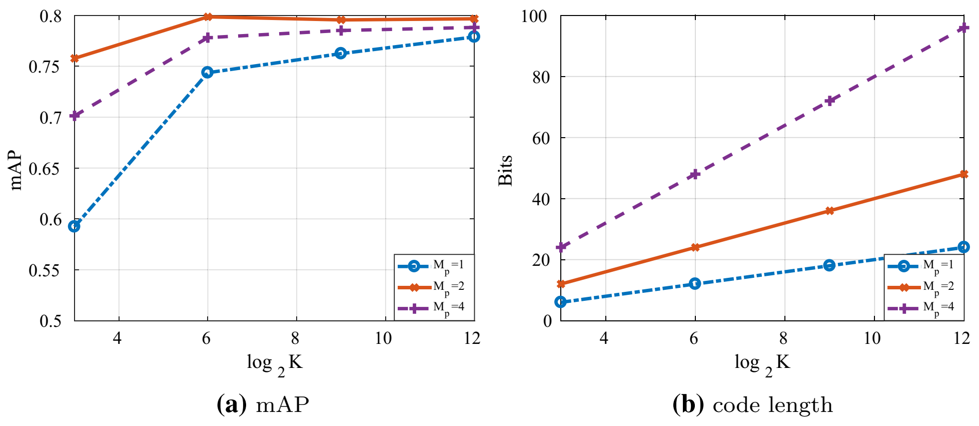

Fig. 4 The influence of M_p

Table 11 mAP comparisons with state-of-the-art methods using 3CNet

Method	12 bits	24 bits	36 bits	48 bits
UBIC (Jain et al. 2017)	0.635	0.672	0.682	0.686
DPQ (Klein and Wolf 2017)	0.673	0.692	0.695	0.693
PQN+CEL	**0.737**	**0.771**	**0.768**	**0.762**
RPQN+CEL	**0.742**	**0.785**	**0.784**	**0.786**
PQN+ATL	**0.741**	**0.782**	**0.787**	**0.786**
RPQN+ATL	**0.758**	**0.799**	**0.796**	**0.797**

Bold values indicate the best performance

Table 12 mAP comparisons with existing state-of-the-art methods using AlexNet base model on the CIFAR10 dataset

Method	16 bits	24 bits	36 bits	48 bits
DRSCH (Zhang et al. 2015)	0.615	0.622	0.629	0.631
DSCH (Zhang et al. 2015)	0.609	0.613	0.617	0.686
DSRH (Zhao et al. 2015)	0.608	0.611	0.617	0.618
VDSH (Zhang et al. 2016)	0.845	0.848	0.844	0.845
DPSH (Li et al. 2015)	0.903	0.885	0.915	0.911
DTSH (Wang et al. 2016b)	0.915	0.923	0.925	0.926
DSDH (Li et al. 2017)	0.935	0.940	0.939	0.939
PQN	**0.947**	**0.947**	**0.946**	**0.947**
RPQN	**0.950**	**0.949**	**0.949**	**0.948**

Bold values indicate the best performance

Table 13 Evaluation on the extremely short code

L	4 bits	6 bits	8 bits	10 bits	12 bits
$M = 1$	0.945	0.945	0.946	0.946	0.946
$M = 2$	0.674	0.882	0.946	0.946	0.947
$M = 4$	0.672	–	0.947	–	0.947

is extremely small, e.g., $L = 4$, the performance of PQN when $M = 1$ significantly outperforms that when $M = 2, 4$. Meanwhile, when $M = 1$, there is not significant performance drop when L decreases from 12 to 4. Note that, when $M = 1$, the proposed PQN achieves a 0.945 mAP when using only 4 bits per code. It considerably outperforms the existing state-of-art method DSDH (Li et al. 2017) which only achieves 0.935 mAP using 16 bits.

6.3 NUS-WIDE

Following the experiment setup in (Wang et al. 2016b; Li et al. 2017), we randomly sample 100 images per class (2100 images in total) as the test query set and the remaining images are used as database images. 500 database images per label are randomly sampled as training images. The mAP is calculated based on the top 5000 returned neighbors. Due to multi-label settings, the cross-entropy loss used in SUBIC (Jain et al. 2017) and the softmax loss in DPQ (Klein and Wolf 2017) are no longer feasible, which explains neither SUBIC (Jain et al. 2017) nor DPQ (Klein and Wolf 2017) conducts the experiments on the NUS-WIDE dataset. Inspired by the success of label embedding proposed in Li et al. (2017), we also adopt a combined loss, which is a weighed sum of our asymmetric triplet loss and a mean square loss defined as

$$\mathcal{L} = \frac{1}{1 + e^{\langle \mathbf{v}, \mathbf{q}_+ \rangle - \langle \mathbf{v}, \mathbf{q}_- \rangle}} + \beta \|\mathbf{W}\mathbf{v} - \mathbf{y}\|_2^2, \qquad (21)$$

where $\mathbf{W}$ represents the weights of an additional fully-connected layer and $\mathbf{y}$ is the label of the sample I. We set $\beta = 10$ by default.

We compare our method with two types of baselines. The first type extracts the features from CNN and then convert the extracted features into binary codes. We directly copy the reported results in Li et al. (2017) which conducts experiments on several traditional hashing methods such as SH (Salakhutdinov and Hinton 2007), ITQ (Gong et al. 2013), KSH (Liu et al. 2012), SDH (Shen et al. 2013), *etc*. The baselines of the second type are deep hashing/quantization methods, where the binary codes are learned in an end-to-end manner. We compare several methods of the second type such as DQN (Cao et al. 2016), DPSH (Li et al. 2015), DTSH (Wang et al. 2016b), DSDH (Li et al. 2017), *etc*. As shown in Table 14, the proposed PQN consistently outperforms these two types of baselines when code length L varies among $\{12, 24, 36, 48\}$. The advantage of our PQN over other methods is more obvious when the code length L is short. For instance, when $L = 24$, our PQN/RPQN achieves a 0.819/0.822 mAP whereas DSDH (Li et al. 2017) only achieves a 0.808 mAP.

6.4 ImageNet100

ImageNet100 (Cao et al. 2017) randomly select 130K images from 100 categories of ImageNet. All images in the validation set as the queries and 100 images per category are selected from the database as the training points. We conduct experiments based on AlexNet backbone and the evaluation metric is mAP@100. We compare with three recent state-of-the-art methods including HashNet (Cao et al. 2017), MIHash (Cakir et al. 2017) and TALR-AP (He et al. 2018). As shown

Table 14 mAP comparisons with existing state-of-the-art methods using AlexNet base model on the NUS-WIDE dataset

Method	12 bits	24 bits	36 bits	48 bits
SH + CNN (Li et al. 2017)	0.621	0.616	0.615	0.612
ITQ + CNN (Li et al. 2017)	0.719	0.739	0.747	0.756
LFH + CNN (Li et al. 2017)	0.695	0.734	0.739	0.759
KSH + CNN (Li et al. 2017)	0.768	0.786	0.790	0.799
SDH+ CNN (Li et al. 2017)	0.780	0.804	0.815	0.824
FASTH+CNN (Li et al. 2017)	0.779	0.807	0.816	0.825
CNNH (Xia et al. 2104)	0.611	0.618	0.625	0.608
NINH (Lai et al. 2015)	0.674	0.697	0.713	0.715
DHN (Zhu et al. 2016)	0.708	0.735	0.748	0.758
DQN (Cao et al. 2016)	0.768	0.776	0.783	0.792
DPSH (Li et al. 2015)	0.752	0.790	0.794	0.812
DTSH (Wang et al. 2016b)	0.773	0.808	0.812	0.824
DSDH (Li et al. 2017)	0.776	0.808	0.820	0.829
PQN	**0.795**	**0.819**	**0.823**	**0.830**
RPQN	**0.797**	**0.822**	**0.829**	**0.831**

The mAP is based on top 5000 nearest neighbors
Bold values indicate the best performance

in Table 15, our PQN and RPQN consistently outperform the compared methods.

7 Experiments on Video Retrieval

We evaluate our method on two public benchmark datasets: UCF101 (Soomro et al. 2012) and HMDB51 (Kuehne et al. 2011). **UCF101** dataset consists of 101 categories containing 13320 total realistic videos. **HMDB51** dataset contains 6766 clips divided into 51 categories, each containing a minimum of 101 clips. Both UCF101 and HMDB51 provide 3 training/testing splits. Following (Liu et al. 2017), we use the third split of UCF101 and first split of the HMDB51. The training data not only is used for training the network but also serves as the reference videos in the database for retrieval. The testing data are the query videos. A reference video is related to the query video if they share the same semantic label.

Backbone network we adopt is an old-fashioned network, BN-Inception (Ioffe and Szegedy 2015), but we remove its last fully-connected layer and softmax layer. To suppress over-fitting, we add a dropout layer with ratio $r = 0.8$ after the last layer of the backbone network. Even though there are many more advanced deep learning architectures available, we select BN-Inception due to the the limitation of our computing resources. Laterly, we will show that the performance achieved by ours using BN-Inception is considerably better than another work (Liu et al. 2017) using a deeper ResNet50 as the backbone. Despite that a temporal stream network taking optical flow as input can achieve higher performance in action retrieval, we do not do that since the baselines we compare only take the RGB frames as input. On both datasets, we set N, the number of sampled frames per video, as 9. The batch size is set to be 128. The initial learning rate is 0.001 and the learning rate will be divided by 10 after every 30 epochs and the training process finishes in 120 epochs. We use SGD as the optimizer and set the momentum as 0.9. The loss function used in training the model is standard cross-entropy loss.

Table 15 Comparisons with state-of-the-art methods on ImageNet100 dataset

	16 bits	32 bits	48 bits
HashNet (Cao et al. 2017)	0.506	0.631	0.663
MIHash (Cakir et al. 2017)	0.569	0.661	0.685
TALR-AP (He et al. 2018)	0.589	0.669	0.699
PQN	**0.613**	**0.682**	**0.707**
RPQN	**0.624**	**0.691**	**0.712**

Bold values indicate the best performance

7.1 Ablation Study

In this section, we conduct ablation study and evaluate the influence of T, M and α on the proposed TPQN, respectively.

7.1.1 Influence of T

We vary T among $\{1, 2, 3\}$. Note that when $T = 1$, it will be equivalent to a one-level global max-pooling. In this case, the temporal product quantization network degenerates to product quantization network. On both datasets, we fix $M = 1$ and increase the number of codewords K from 32 to 2048.

As shown in Fig. 5, when $T = 2, 3$, it consistently outperform that when $T = 1$, which validates the advantage of the proposed temporal product quantization network over product quantization network. Nevertheless, a higher T will take more bits, leading to a higher memory and computation cost. To balance the precision and efficiency, we set $T = 2$ by default on both datasets. Meanwhile, from Fig. 5 we can also observe that as K increases, the mAP increases in the early stage and then drops. The increase of mAP is due to that a higher K is capable of representing richer information. In contrast, the mAP decreases when $K > 128$ is caused by over-fitting. We will show in Sect. 7.2 that the quantization can serve as a regularization mechanism which suppresses the over-fitting. How to select K is dependent on the scale of the dataset. As a rule of thumb, we pick a larger K for a larger dataset. As shown in Fig. 5, when T varies among $\{1, 2, 3\}$, it consistently achieves the best performance when $K = 128$ on UCF101 dataset and when $K = 64$ on HMDB51 dataset.

7.1.2 Influence of *M*

A larger M brings a richer codebook as well as a greater complexity. We vary M among $\{1, 2, 4\}$. On both datasets, we set $T = 2$ and increase K from 32 to 2048. In this scenario, the number of bits required for representing a video is $3Mlog_2K$. As shown in Fig. 6, when K is small, $M = 2, 4$ achieves much better performance than $M = 1$, this is expected since a small K will have a limited capability of representing and therefore need a larger M to enrich the codewords. On the contrary, when K is large, the advantage of $M = 2, 4$ over $M = 1$ is not so obvious. Meanwhile, in consistency with the previous experimental results shown in Fig. 6, when M varies among $\{1, 2, 4\}$, it continuously achieves the highest precision on UCF101 dataset when $K = 128$ and on HMDB51 when $K = 64$.

7.1.3 Influence of *α*

α controls the consistency between the approximation function $f_{tm}(\cdot, \alpha)$ and original quantization function $q_{tm}(\cdot)$. We fix $T = 2$ and $M = 2$ and test our TPQN by increasing α from 2 to 10 and vary K among $\{32, 64, 128\}$. As shown in Fig. 7, the performance, when α is within the range $[5, 10]$, the performance of TPQN is considerably stable. Nevertheless, we can observe a significant performance drop when α decreases from 5 to 2. This drop is due to the fact that a small α brings a large inconsistency between the approximation function $f_{tm}(\cdot, \alpha)$ in the training phase and the hard quanti-

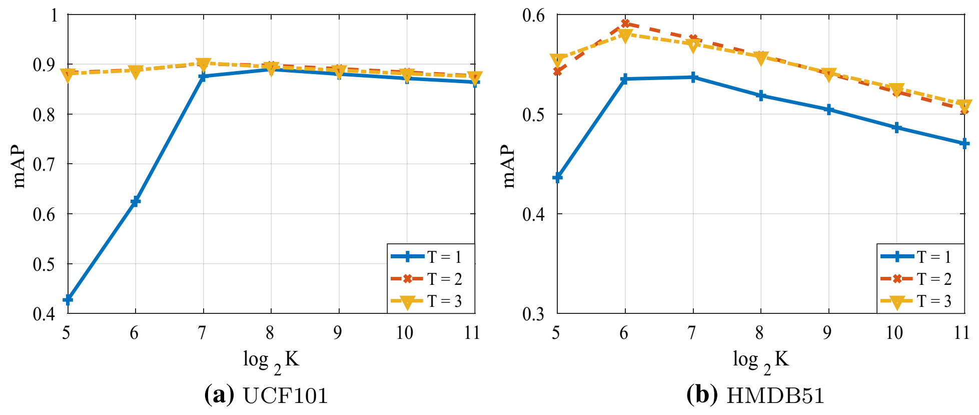

Fig. 5 The influence of T

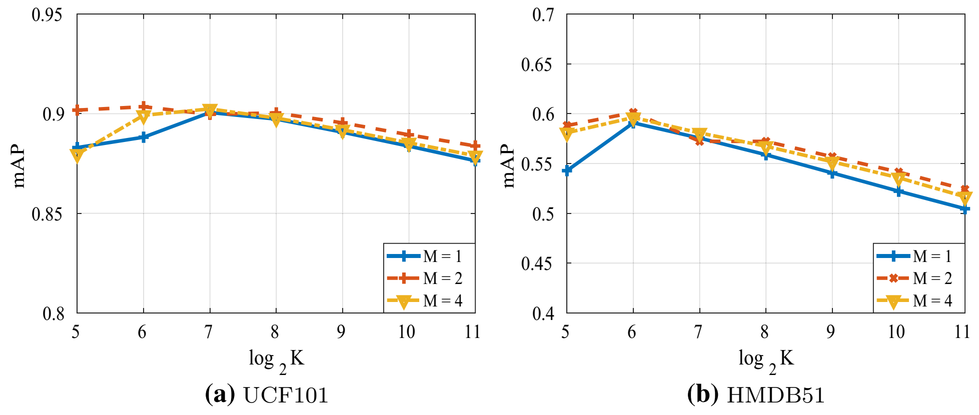

Fig. 6 The influence of M

Fig. 7 The influence of α

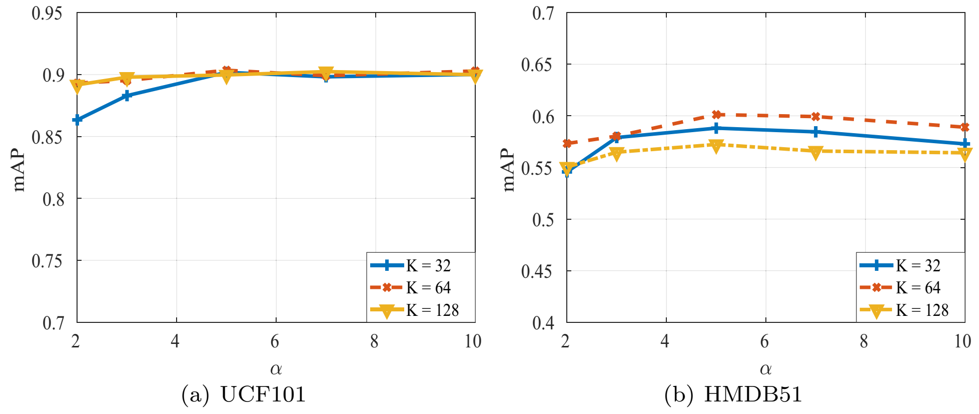

zation in the indexing phase. Meanwhile, on the HMDB51 dataset, we also observe a slight performance drop when α increases from 7 to 10. This performance drop is caused by the fact that a large α will tend to make the training unstable. By default, we set $\alpha = 5$ on both datasets.

7.1.4 Action Recognition

We also evaluate the performance of the proposed TPQN for action recognition. To be specific, we also the nearest neighbor classifier for recognition. We compare with TSN (Wang et al. 2016a), using the same backbone network, BN-Inception (Ioffe and Szegedy 2015). To make a fair comparison, both ours and TSN only take RGB frames as input and do not use optical flows. As shown in Table 19, benefited from temporal pyramid pooling, our TPQN considerably outperforms TSN in the action recognition.

7.2 Complexity Analysis and Regularization

In this section, we analyze the complexity reduction brought by quantization and also show the regularization functionality of the quantization. We will show that our TPQN not only significantly boosts the efficiency but also serves as a regularization mechanism, improving the precision. To make a fair comparison, we compare with a baseline by directly removing the quantization operation, *i.e.*, the third step in temporal product quantization layer and keep other parts of TPQN fixed. As for our TPQN, we set $M = 2$ and $K = 64$ on both datasets.

Without quantization, the video features are high-dimension real-value vectors. For instance, when $T = 2$, the feature dimension is $D(T + 1) = 1024 \times 3 = 3072$ and it takes $3072 \times 4 = 12288$ bytes to store the feature in a float-type array. In contrast, using the quantization, it only takes $(T + 1)M\lceil log_2 K/8\rceil = 6$ bytes, achieving an approximate $2000\times$ memory reduction.

Table 16 Regularization function of the product quantization structure

	UCF101			HMDB51		
Quantization?	$T = 1$	$T = 2$	$T = 3$	$T = 1$	$T = 2$	$T = 3$
NO	0.8547	0.8642	0.8622	0.4628	0.4927	0.4945
YES	0.8639	0.9035	0.9023	0.5352	0.6012	0.5801

Table 17 Comparison with existing hashing methods

	UCF101				HMDB			
	6 bits	12 bits	18 bits	36 bits	6 bits	12 bits	18 bits	36 bits
LSH	0.090	0.220	0.326	0.521	0.068	0.116	0.149	0.231
SH	0.234	0.448	0.613	0.777	0.155	0.255	0.344	0.440
ITQ	0.282	0.588	0.728	0.828	0.206	0.360	0.449	0.521
SPBE	0.266	0.532	0.717	0.805	0.209	0.327	0.408	0.512
KSH	0.450	0.752	0.842	0.878	0.325	0.436	0.532	0.572
DSH	0.513	0.807	0.856	0.882	0.331	0.457	0.546	0.586
Unsupervised PQ	0.562	0.831	0.862	0.891	0.485	0.533	0.568	0.582
Ours	0.626	0.864	0.888	0.904	0.535	0.563	0.591	0.601

Table 18 Comparison with deep video hashing methods

	SUBIC (Jain et al. 2017)			DHCM (Liu et al. 2017)			TPQN (Ours)		
	64	128	256	64	128	256	12	18	36
UCF101	0.324	0.432	0.449	0.759	0.817	0.843	0.864	0.888	0.904
HMDB51	0.192	0.247	0.298	0.356	0.367	0.368	0.563	0.591	0.601

Table 19 The performance in action recognition

	UCF101	HMDB51
TSN (Wang et al. 2016a)	85.3	51.0
Ours	90.9	62.3

Meanwhile, we find the quantization also significantly improves the retrieval precision as shown in Table 16. This is due to the regularization mechanism brought by the quantization, which suppresses overfitting and improves the generalization capability of the trained model. For instance, when $T = 2$, our TPQN achieves 0.9035 mAP on UCF101 dataset and 0.6012 mAP on HMDB51 dataset. In contrast, after removing the quantization, it only achieves 0.8642 mAP on UCF101 dataset and 0.4927 mAP on HMDB51 dataset.

7.3 Comparison with State-of-the-Art Methods

To further demonstrate the effectiveness of the proposed TPQN, we compare it with the state-of-the-art methods. The compared methods can be categorized into two types. The first type of methods are based on a two-step process: video feature extraction followed by hashing. To make a fair comparison, we directly use the features without quantization used in Table 16 for hashing. We implement multiple hashing methods including LSH (Datar et al. 2004), SH (Weiss et al. 2009) , ITQ (Gong et al. 2013), SPBE (Xia et al. 2015), KSH (Liu et al. 2012), SDH (Shen et al. 2015). Among them, LSH (Datar et al. 2004), SH (Weiss et al. 2009) , ITQ (Gong et al. 2013) and SPBE (Xia et al. 2015) are unsupervised hashing methods, whereas KSH (Liu et al. 2012) and SDH (Shen et al. 2015) are supervised hashing methods. Meanwhile, we also compare with unsupervised PQ. As show in Table 17, our method consistently outperforms other methods on both UCF101 and HMDB51 datasets, especially when bit length is small. For instance, on UCF101 dataset, our method achieves a 0.864 mAP when bit length is only 12 whereas the second best DSH only achieves a 0.807 mAP using the same bit length. On HMDB51 dataset, our method achieves a 0.535 mAP when bit length is only 12 whereas the second best DSH only achieves a 0.331 mAP.

The second type of methods is deep video hashing. We mainly compare with two most recent methods, SUBIC (Jain et al. 2017) and Deep Hashing with Category Mask (DHCM) (Liu et al. 2017). Note that even if SUBIC and DHCM are based on a deeper ResNet50 backbone, our result consistently outperforms both of them using a shallower backbone BN-Inception as show in Table 18. To be specific, on the UCF101 dataset, we achieve a 0.904 mAP using only 36 bits, whereas DHCM only achieves a 0.843 using 256 bits. Meanwhile, on the HMDB51 dataset, we achieve a 0.563 mAP using only 12 bits, whereas DHCM only achieves a 0.368 using 256 bits (Table 19).

8 Conclusion

In this paper, by constructing an approximate function, we make the product quantization differentiable and feasible to be incorporated in a neural network. Product quantization nework (PQN) is introduced, which learns a discriminative and compact image representation in an end-to-end manner. Asymmetric triplet loss extended from triplet loss is introduced, which directly optimizes the representation's adaptability to retrieval based on asymmetric distance. By revisiting residual quantization, we extend PQN to residual product quantization (RPQN) which triggers the residual learning and further improves the discriminativeness of the representation. Moreover, by exploiting the temporal consistency inherited in videos, we extend PQN to temporal product quantization network (TPQN) for fast video retrieval. Interestingly, our experiments show that the product quantization not only improves the retrieval efficiency but also improves the model's generalizability and retrieval accuracy. Systematic experiments conducted on benchmark datasets demonstrate state-of-the-art performance of the proposed PQN, RPQN and TPQN in fast image and video retrieval.

Acknowledgements This work is supported in part by a gift grant from Adobe and startup funds from University at Buffalo.

References

Babenko, A., & Lempitsky, V. (2014). Additive quantization for extreme vector compression. In *CVPR* (pp. 931–938).

Babenko, A., & Lempitsky, V. (2015). Aggregating local deep features for image retrieval. In *ICCV* (pp. 1269–1277).

Babenko, A., Slesarev, A., Chigorin, A., & Lempitsky, V. (2014). Neural codes for image retrieval. In *ECCV* (pp. 584–599). Berlin: Springer.

Bai, S., Bai, X., Tian, Q., & Latecki, L. J. (2018). Regularized diffusion process on bidirectional context for object retrieval. *TPAMI*.

Bai, S., Zhou, Z., Wang, J., Bai, X., Latecki, L. J., & Tian, Q. (2017). Ensemble diffusion for retrieval.

Cakir, F., He, K., Bargal, S. A., & Sclaroff, S. (2017). Mihash: Online hashing with mutual information. In *ICCV*.

Cao, L., Li, Z., Mu, Y., & Chang, S. F. (2012). Submodular video hashing: a unified framework towards video pooling and indexing. In *Proceedings of the 20th ACM international conference on Multimedia* (pp. 299–308). ACM.

Cao, Y., Long, M., Wang, J., Zhu, H., & Wen, Q. (2016). Deep quantization network for efficient image retrieval. In *AAAI*.

Cao, Z., Long, M., Wang, J., & Yu, P. S. (2017). Hashnet: Deep learning to hash by continuation. In *ICCV*.

Charikar, M. S. (2002). Similarity estimation techniques from rounding algorithms. In *Proceedings of the 34th annual ACM symposium on theory of computing* (pp. 380–388).

Chen, Y., Guan, T., & Wang, C. (2010). Approximate nearest neighbor search by residual vector quantization. *Sensors*, *10*(12), 11259–11273.

Chua, T. S., Tang, J., Hong, R., Li, H., Luo, Z., & Zheng, Y. (2009). Nus-wide: a real-world web image database from national university of singapore. In *Proceedings of the ACM international conference on image and video retrieval* (p 48).

Datar, M., Immorlica, N., Indyk, P., Mirrokni, V. S. (2004). Locality-sensitive hashing scheme based on p-stable distributions. In *Proceedings of the twentieth annual symposium on Computational geometry* (pp. 253–262).

Ge, T., He, K., Ke, Q., & Sun, J. (2013). Optimized product quantization for approximate nearest neighbor search. In *CVPR* (pp. 2946–2953). IEEE.

Gong, Y., Lazebnik, S., Gordo, A., & Perronnin, F. (2013). Iterative quantization: A procrustean approach to learning binary codes for large-scale image retrieval. *IEEE T-PAMI*, *35*(12), 2916–2929.

Gordo, A., Almazán, J., Revaud, J., & Larlus, D. (2016). Deep image retrieval: Learning global representations for image search. In *ECCV* (pp. 241–257). Springer.

He, K., Cakir, F., Bargal, S. A., & Sclaroff, S. (2018). Hashing as tie-aware learning to rank. In *CVPR*.

He, K., Zhang, X., Ren, S., & Sun, J. (2016). Deep residual learning for image recognition. In: *Proceedings of the IEEE conference on computer vision and pattern recognition* (pp. 770–778).

Hong, W., Meng, J., & Yuan, J. (2018). Distributed composite quantization. In *AAAI*.

Hong, W., Meng, J., & Yuan, J. (2018). Tensorized projection for high-dimensional binary embedding. In *AAAI*.

Hong, W., & Yuan, J. (2018). Fried binary embedding: From high-dimensional visual features to high-dimensional binary codes. *IEEE Transactions on Image Processing*, *27*(10), 1.

Hong, W., Yuan, J., & Bhattacharjee, S. D. (2017). Fried binary embedding for high-dimensional visual features. *CVPR*, *11*, 18.

Ioffe, S., & Szegedy, C. (2015). Batch normalization: Accelerating deep network training by reducing internal covariate shift. In *International conference on machine learning* (pp. 448–456).

Jain, H., Zepeda, J., Perez, P., & Gribonval, R. (2017). Subic: A supervised, structured binary code for image search. In *ICCV* (pp. 833–842).

Jegou, H., Douze, M., & Schmid, C. (2011). Product quantization for nearest neighbor search. *IEEE T-PAMI*, *33*(1), 117–128.

Jégou, H., Douze, M., Schmid, C., & Pérez, P. (2010). Aggregating local descriptors into a compact image representation. In: *CVPR* (pp. 3304–3311).

Jiang, Q. Y., & Li, W. J. (2018). Asymmetric deep supervised hashing. *AAAI*.

Klein, B., & Wolf, L. (2017). In defense of product quantization. arXiv preprint arXiv:1711.08589.

Krizhevsky, A. (2009). Learning multiple layers of features from tiny images.

Kuehne, H., Jhuang, H., Garrote, E., Poggio, T., & Serre, T. (2011). Hmdb: a large video database for human motion recognition. In *IEEE International Conference on Computer Vision (ICCV), 2011* (pp. 2556–2563). IEEE.

Lai, H., Pan, Y., Liu, Y., & Yan, S. (2015). Simultaneous feature learning and hash coding with deep neural networks. arXiv preprint arXiv:1504.03410.

Li, Q., Sun, Z., He, R., & Tan, T. (2017). Deep supervised discrete hashing. In *NIPS* (pp. 2479–2488).

Li, W. J., Wang, S., & Kang, W. C. (2015). Feature learning based deep supervised hashing with pairwise labels. arXiv preprint arXiv:1511.03855

Liong, V. E., Lu, J., Tan, Y. P., & Zhou, J. (2017). Deep video hashing. *IEEE Transactions on Multimedia*, *19*(6), 1209–1219.

Liu, H., Wang, R., Shan, S., & Chen, X. (2016). Deep supervised hashing for fast image retrieval. In *CVPR* (pp. 2064–2072).

Liu, W., Wang, J., Ji, R., Jiang, Y. G., & Chang, S. F. (2012). Supervised hashing with kernels. In *2012 IEEE Conference on Computer Vision and Pattern Recognition* (pp. 2074–2081). IEEE.

Liu, X., Zhao, L., Ding, D., & Dong, Y. (2017). Deep hashing with category mask for fast video retrieval. CoRR arXiv:1712.08315.

Martinez, J., Clement, J., Hoos, H. H., & Little, J. J. (2016). Revisiting additive quantization. In *European Conference on Computer Vision* (pp. 137–153). Springer.

Ng, J.Y.H., Yang, F., Davis, L. S. (2015). Exploiting local features from deep networks for image retrieval. arXiv preprint arXiv:1504.05133.

Norouzi, M., & Fleet, D. J. (2013). Cartesian k-means. In *CVPR* (pp. 3017–3024).

Norouzi, M., Fleet, D. J., & Salakhutdinov, R. R. (2012). Hamming distance metric learning. In *Advances in neural information processing systems* (pp. 1061–1069).

Perronnin, F., Liu, Y., Sánchez, J., & Poirier, H. (2010). Large-scale image retrieval with compressed fisher vectors. In *CVPR* (pp. 3384–3391).

Philbin, J., Chum, O., Isard, M., Sivic, J., & Zisserman, A. (2007). Object retrieval with large vocabularies and fast spatial matching. In *CVPR* (pp. 1–8).

Sablayrolles, A., Douze, M., Jégou, H., & Usunier, N. (2017). How should we evaluate supervised hashing? In *ICASSP*.

Salakhutdinov, R., & Hinton, G. (2007). Semantic hashing. *RBM*, *500*(3), 500.

Shen, F., Shen, C., Liu, W., & Shen, H. T. (2013). Supervised discrete hashing. *IEEE T-PAMI*, *35*(12), 2916–2929.

Shen, F., Shen, C., Liu, W., & Shen, H. T. (2015). Supervised discrete hashing. In: *CVPR* (Vol. 2, p. 5).

Soomro, K., Zamir, A. R., & Shah, M. (2012). Ucf101: A dataset of 101 human actions classes from videos in the wild. arXiv preprint arXiv:1212.0402.

Tu, Z., Li, H., Zhang, D., Dauwels, J., Li, B., & Yuan, J. (2019). Action-stage emphasized spatio-temporal VLAD for video action recognition. *IEEE Transactions on Image Processing*.

Tu, Z., Xie, W., Qin, Q., Veltkamp, R. C., Li, B., & Yuan, J. Multi-stream cnn: Learning representations based on human-related regions for action recognition. *Pattern Recognition*.

Wang, L., Xiong, Y., Wang, Z., Qiao, Y., Lin, D., Tang, X., & Van Gool, L. (2016a). Temporal segment networks: Towards good practices for deep action recognition. In *European Conference on Computer Vision* (pp. 20–36). Springer.

Wang, X., Shi, Y., & Kitani, K. M. (2016b). Deep supervised hashing with triplet labels. In *ACCV* (pp. 70–84). Springer.

Wang, X., Zhang, T., Qi, G.J., Tang, J., & Wang, J. (2016c). Supervised quantization for similarity search. In *CVPR* (pp. 2018–2026).

Weiss, Y., Torralba, A., & Fergus, R. (2009). Spectral hashing. In *NIPS* (pp. 1753–1760).

Wu, C.Y., Manmatha, R., Smola, A. J., & Krähenbühl, P. (2017a). Sampling matters in deep embedding learning. In *ICCV*.

Wu, G., Liu, L., Guo, Y., Ding, G., Han, J., Shen, J., & Shao, L. (2017b). Unsupervised deep video hashing with balanced rotation. In *IJCAI*.

Xia, R., Pan, Y., Lai, H., Liu, C., & Yan, S. (2014). Supervised hashing for image retrieval via image representation learning. In *AAAI* (pp. 2156–2162). AAAI Press.

Xia, Y., He, K., Kohli, P., & Sun, J. (2015). Sparse projections for high-dimensional binary codes. In *Proceedings of the IEEE conference on computer vision and pattern recognition* (pp. 3332–3339).

Ye, G., Liu, D., Wang, J., & Chang, S. F. (2013). Large-scale video hashing via structure learning. In Proceedings of the IEEE International Conference on Computer Vision (pp. 2272–2279).

Yu, T., Meng, J., & Yuan, J. (2017a). Is my object in this video? reconstruction-based object search in videos. In *Proceedings of the 26th International Joint Conference on Artificial Intelligence* (pp. 4551–4557). AAAI Press.

Yu, T., Wang, Z., & Yuan, J. (2017b). Compressive quantization for fast object instance search in videos. In *ICCV* (pp. 833–842).

Yu, T., Wu, Y., Bhattacharjee, S. D., & Yuan, J. (2017c). Efficient object instance search using fuzzy objects matching. In *AAAI*.

Yu, T., Wu, Y., & Yuan, J. (2017d). Hope: Hierarchical object prototype encoding for efficient object instance search in videos. In *Proceedings of the IEEE conference on computer vision and pattern recognition* (pp. 2424–2433).

Yu, T., Yuan, J., Fang, C., Jin, H. (2018). Product quantization network for fast image retrieval. In *Proceedings of the European Conference on Computer Vision (ECCV)* (pp. 186–201).

Zhang, R., Lin, L., Zhang, R., Zuo, W., & Zhang, L. (2015). Bit-scalable deep hashing with regularized similarity learning for image retrieval and person re-identification. *IEEE TIP*, *24*(12), 4766–4779.

Zhang, T., Du, C., & Wang, J. (2014). Composite quantization for approximate nearest neighbor search. In *ICML, 2* (pp. 838–846).

Zhang, Z., Chen, Y., & Saligrama, V. (2016). Efficient training of very deep neural networks for supervised hashing. In *CVPR* (pp. 1487–1495).

Zhao, F., Huang, Y., Wang, L., & Tan, T. (2015). Deep semantic ranking based hashing for multi-label image retrieval. In *CVPR* (pp. 1556–1564).

Zhu, H., Long, M., Wang, J., & Cao, Y. (2016). Deep hashing network for efficient similarity retrieval. In *AAAI*.